Critical *J*-integral based fracture toughness of 15-5PH after different heat treatment history

Jikai.Liu[1*], Michel.Coret[1] and Alain Combescure[1]

[1] Université de Lyon, CNRS INSA-Lyon,

LaMCoS (Laboratoire de Mécanique des Contacts et des Structures) UMR5259, F-69621, France

[*] jikai.liu@insa-lyon.fr

Keywords: Fracture toughness, Phase transformation, Critical *J*-integral, Boundary condition, Digital image correlation.

Abstract. Our investigation proposes a simple and effective method to extract the elastoplastic fracture toughness J_{1C} from a simple experiment on a Single Edge Notched Plate (SENP). The method is based on a combination of global experimental load displacement measurements, finite element simulation, and Digital Image Correlation (DIC) which is used to observe the crack tip motion as well as to determine the appropriate Boundary Conditions (BC) to be applied in numerical simulation. The method is applied to obtain the J_{1C} value of 15-5PH after different heat treatment histories, which can represent the influence of the different material state history on the mechanical properties due to the heat treatment and possible phase transformation. The result of J_{1C} value shows that the pure martensite 15-5PH has higher fracture toughness at room temperature than at 200°C. The toughness is also higher than the original material after one cycle heat treatment which is probably caused by some stable residual austenite. Meanwhile, pure austenite 15-5PH has a higher fracture toughness than pure martensite 15-5PH at 200°C. The J_{1C} value of the dual phase 15-5PH during the martensitic transformation also shows that austenite can enhance the ductility of the material as well as fracture toughness.

1. Introduction

Crack curing is attractive due to less expensive for life extension for expensive components, but it is very often not chosen for important components because people fear the consequences of this reparation on the future safety of the cured component. The main reason is that there is a lack of understanding about the effects of reparation in this type of situation. If the crack root is still present after curing, what happens to this initial damage during the repair (filling with welding material)? This research is devoted to the acquisition of basic understanding of what happens in such cases. It is focused on getting basic information on the fracture material properties in case of typical repair and refilling temperature histories. The following experimental tests are performed. A fatigue crack side is initiated in a thin plate. This plate is submitted to a typical uniform thermal history and the monotonic load crack propagation tests are performed on the plate. The objective of these tests is to evaluate if the toughness is affected by the temperature history and how much. The particular material chosen (15-5PH) is a dual phase material which experiences phase transformation:

dilatometry tests permit to characterize this transformation. The evolution of standard material properties as yield stress or Young's modulus under the same thermal history is evaluated using standard round bar monotonic testing.

1.1 Stainless steel: 15-5PH

The material 15-5PH (Condition H1025) is considered herein. 15-5PH is a martensitic precipitation hardening stainless steel which is a precipitation of age hardened and heat solution-treated material at 1025°F for 4 hours and then air cooling. It is widely used in aerospace and nuclear areas due to it's high toughness, hardness and good corrosion resistance as well [1]. The following table shows the chemical composition of 15-5PH.

Table 1. Chemical compositions of 15-5PH

Element	Cr	Ni	Cu	C	Mn	Other alloys	Fe
wt%	15.44	4.50	3.16	0.02	0.66	*N/A*	Balance

1.2 Phase transformation in 15-5PH

Like others metals, 15-5PH experiences phase transformation during specific heat treatment. This material is in the family of dual phase ones because it only experiences austenite and martensitic transformation but no ferrite or pearlite transformation. Figure 1 displays the elongation curve of 15-5PH with a whole heat treatment cycle.

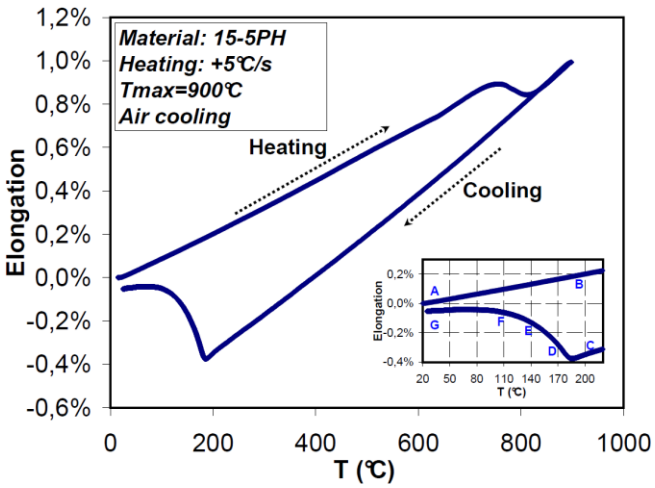

Fig. 1. Elongation during a heat treatment cycle.

The test is done with an initial heating rate of +5°C/s until the maximum temperature 900°C. The first linear response is the expansion of martensite. At about 770°C the austenite transformation starts and is finished at about 815°C. After the maximum temperature, the specimen is air-cooled. The first part of the decreasing curve is the linear contraction of austenite which stops at about 185°C where martensitic transformation starts. The transformation completes at about 40°C.

We will focus on the martensitic transformation of 15-5PH to study the effect of metallurgical phase transformation on mechanical behaviour. One can read in [2] that the martensitic transformation of 15-5PH is cooling temperature driven, that is to say, once the temperature stops decreasing the transformation will also stop. Our experimental results are consistent with this observation. This means that one can keep a constant phase proportion if the temperature is not changed during the martensitic transformation and do the corresponding mechanical test.

In the lower right corner of fig.1, seven points (A to G) are marked where we will study the mechanical behaviour. For example point A and G are two tests performed at room temperature one before the heat treatment (A) and another after a whole cycle heat treatment (G). Point B is fully

martensite at 200°C while point C is totally austenite at the same temperature just before the martensitic transformation; Point D, E and F are three points during the martensitic transformation at 170, 140 and 110°C. Table 2 shows the phase proportion at each point [1][3][4][5].

Table 2. Analysis points related to the phase

Point	A	B	C	D	E	F	G
Phase	α	α	γ	α/γ	α/γ	α/γ	α
% of α	100%	100%	≈0%	25%	60%	80%	≈100%

Note: α presents martensite, γ presents austenite, α/γ means martensite and austenite mixed. The reason why there are two pproximately equal symbol ≈ is that the phase transformation may be not finished completely, for example there may be some residual austenite exists at point G.

1.3 Effect of phase transformation on crack resistance

A lot of works have been done about the effect of phase transformation on material properties in the last half century. Greenwood, Johnson and Magee respectively worked on the effect of an applied stress during the phase transformation: they showed that this stress could lead to an additional irreversible strain [6][7], described by the phase TRansformation Induced Plasticity(TRIP). Further more, J.P.Bressanelli and A.Moskowitz presented that TRIP can increase the strain-hardening rate which results in an overall increase of tensile strength and uniform ductility [8]. Consequently the TRIP high strength steel came out [9]. Subsequently many papers appeared dealing with the influence of mechanically-induced martensitic transformation on the general mechanical behaviour of metastable austenitic steels under monotonic and cyclic loading [10]. The phase transformation in shape memory alloys (SMAs) which involves negative volumetric change, would result in an increase in the crack-tip stress-intensity factor and thus a decrease in fracture toughness [11]. More investigation results could be found in [12-17]. In our paper, we will present the fracture toughness values before, during and after the martensitic transformation of 15-5PH. This will provide an input for the effect of phase transformation in 15-5PH on its crack propagation resistance.

1.4 Critical *J*-integral evaluation

Rice [18], Begley and Landes [19], and others [20] showed that the energy rate interpretation of the *J*-integral is fundamental to elastic–plastic fracture toughness testing [21]. Crack propagation initiates once the loading attains a material-dependent critical J-integral value J_{1C}. In the last several decades, several formulas have been proposed based of great quantity of experiments on different specimen with different geometry. In 1981, American Electric Power Research Institute (EPRI) presented some equations for calculating critical *J*-integral which takes into account of the material hardening exponent [22]. But if the material hardening exponent is too big, the EPRI solution is difficult to apply. American Society for Testing and Materials, also stated the standard test method for measurement of fracture toughness J_{1C} in 1996 [23]. Another well known experimental method proposed by Begley and Landes [19][24] for the determination of J_{1C} which is based on the comparison of load-displacement curves for two specimens with same geometry which differ by the crack lengths a and $a+da$.

However all these methods need nevertheless many experiments and the dependence of the toughness to the finite *da* has to be studied which means a large quantity of experiments. Furthermore, this method is based on the basic assumption of having the same boundary conditions between all the experiments. Every one knows that this condition is really strong. The experiments have also to be done on specific geometries which increase a lot the costs of the experiments.

It was then decided to extract the J_{1C} value using an alternative method which combines experiments, DIC and numerical simulation of the tests. We first of all apply systematically Digital

Image Correlation (DIC), a full-field image analysis and a non-contact measurement method [25][26]. The experimental global load displacement curve is used to determine the crack propagation starting point. It was observed using the pictures of the experiments obtained by DIC (compared in case of room temperature with Johnson method for crack length measurement [27]) that crack propagation initiated just after the maximum load. The DIC was then used to find the real Boundary Conditions (BC) to be applied to the finite element model for any fracture tests for each load level. The test has then been simulated by a refined finite element plane stress analysis, using the material properties extracted from the standard stress strain curve obtained at the corresponding thermal history. The FEM predicted load displacement curve is compared to the experimental one to check the quality of the simulation. J_{1C} value is then extracted fro all points from A to G using the elastoplastic evaluation of *J*.

2. Experiments

2.1 Specimen preparation

The geometric parameters of the Single Edge Notched Plate (SENP) and round bar specimen are presented in fig. 2. About the SENP, the two big holes are used to fix the sample, and the two small holes allow to input the current and produce a controlled fatigue crack using Potential Drop (PD) technology. The notch has been enlarged in the figure 2 and precisely defined in Detail B. The fatigue crack length is deduced by the PD method using Johnson's formula [27].

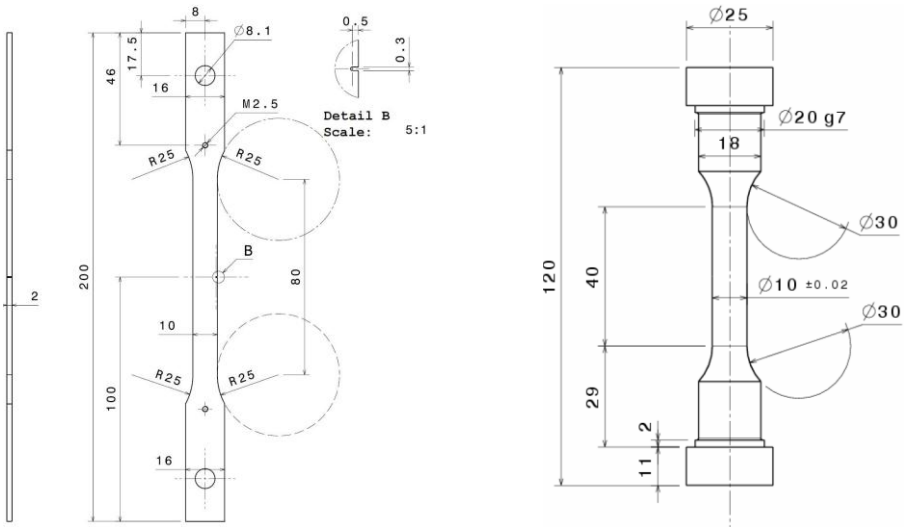

Fig. 2. Round bar (right one) and single edge notched specimen (all dimensions in mm)

2.2 Experimental devices

The fracture test devices are presented in this section. A servo-electro-hydraulic tension-compression machine with maximum capacity of 250KN is employed. The strain is measured by an extensometer. The type K thermal couples are connected to a converter for signal amplification and conversion. The force, strain and temperature signals are collected by a digital acquisition system. Heating is generated by electromagnetic induction, and power is supplied by a 3KW generator. The automated configuration includes the controller, a PC, and the system software bundle. Fig.3 shows a global view of the experiment. For DIC, two cameras were placed in front of each face of the specimen to record digital images of the two sample surfaces. The zone of interest (ZOI) is chosen in the reference photo. In order to obtain good digital image of the ZOI, good illumination condition,

spray paint and proper speckle pattern have been carefully chosen. Device for round specimen here is neglected which is very similar to we introduced for the fracture tests.

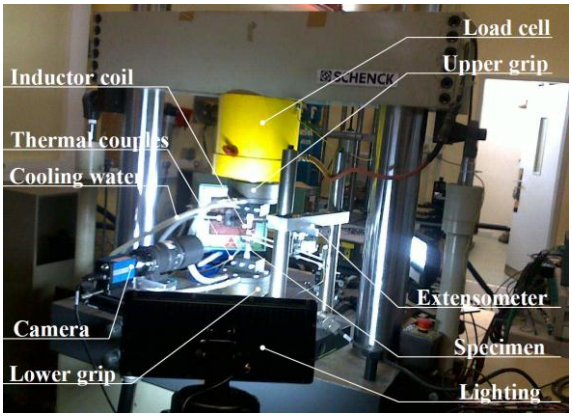

Fig. 3. Experiment device and it's installation

2.3 Experimental process

1) Do the tensile tests of round bar to find the basic mechanical parameters for simulation;
2) Produce the expected fatigue crack with PD method and Johnson's formula;
3) Do the fracture test for the chosen seven points (A, B, C, D, E, F and G) on the pre-cracked specimen with uniaxial displacement controlled loading (displacement rate 0.5mm/minute)
4) During the uniaxial fracture test, take the photos (5 pictures / second) of the ZOI.

3. Experimental result and analysis

3.1 Tensile tests result

The tensile tests were done on the round bar specimen at seven points. The stress-strain curves are shown in figure 4(a) where we can find that the ultimate stress and young's modulus at point G are smaller then original material which is point A. Comparing the pink and yellow curve, the pure austenite at 200°C is more ductile but lower strength than pure martensite at the same temperature. For point D, E and F, as more austenite transformed to martensite and temperature decreasing, the material has a more higher strength and much bigger elastic modulus. The difference between A, B and other five points is A and B have a majority period of elastic strain before damage while other fives have the majority plastic strain.

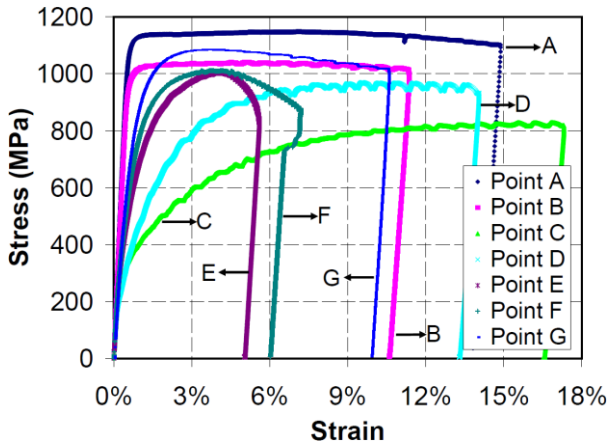

(a) Stress-strain curves

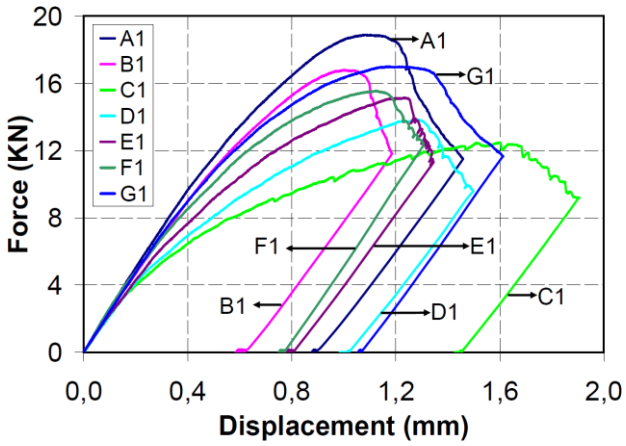

(b) Loading-displacement curve

Fig. 4. Mechanical test results of 15-5PH after different heat treatment history

3.2 Fatigue crack fabrication

For each testing conditions (points A to G) at least two samples with different pre-crack length were produced. Johnson's formula, DIC, and visual microscope observation were used to get the mean value of fatigue crack length a.

3.3 Force vs. displacement curves of uniaxial fracture tests

Table 3 displays the maximum load obtained for each cracked specimen which contains the pre-crack length of every fracture sample.

Table 3. Result of fracture tests

Experimental Point	Temperature [°C]	Sample	Fatigue initial crack length [a ,mm]	Maximum force of the fracture test [KN]
A	20	A1	1,654	18,87
		A2	2,060	18,51
B	200	B1	1,579	16,78
		B2	1,264	16,73
C	200	C1	1,587	11,85
		C2	2,504	10,47
D	170	D1	1,557	13,83
		D2	2,486	11,67
E	140	E1	1,566	15,12
		E2	1,249	16,33
F	110	F1	1,693	15,54
		F2	1,265	16,93
G	20	G1	1,571	16,99
		G2	1,260	17,41

Force vs. global displacement curves of the specimens which have the similar initial crack length are plotted in the figure 4(b). The abscissa and ordinate values are given by the electro-mechanical testing machine.

One may be surprised that the maximum force of the samples with different crack length are not always consistent with the initial crack length. The reason has been found to be due to a difficult control of the “grip” conditions of the specimen into the machine. This difficulty is created by the extremely simple design of the specimen but has been solved using DIC and finite element simulation of the experiments.

3.4 Extract boundary conditions from DIC for the FEM simulation

Let us illustrate the method on specimen A1. The first point is to decide the crack propagation initial point: it was found by comparison of DIC photos and potential drop method on room temperature experiments that this point is determined by the maximum load.

Icasoft software [28] was then used to process the initial and following pictures to find the displacement field in the loading direction on top (E-PE line) and bottom (F –PF line) of the ZOI for each load step.

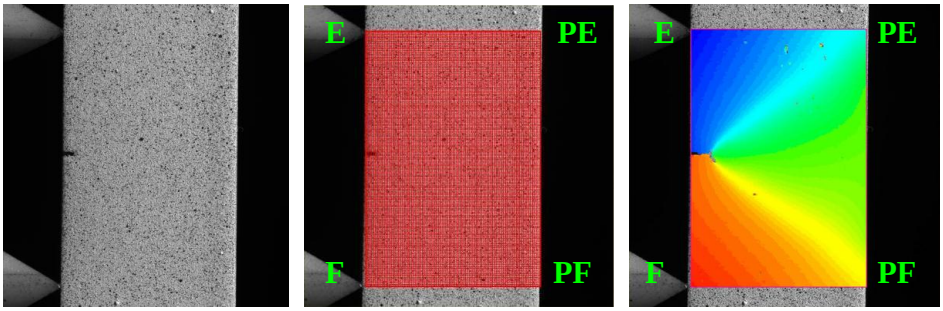

(a) (b) (c)

Fig. 5. vertical displacements fields obtained from DIC for specimen A1

In fig.5, (a) shows the reference photo of pre-cracked specimen, the fatigue crack is difficult to see even there is no paint on the surface; (b) shows the ZOI (E-PE-F-PF), its length is 15mm which is also the distance between the two pins of the extensometer, its width is equal to the width of the sample which is 10mm; (c) displays the displacement filed in loading direction (vertical) obtained from DIC.

DIC analysis permits to extract displacement fields along lines E-PE as well as F-PF for each picture. Fig .6(a) displays the displacement obtained by DIC at the maximum force along lines E-PE and F-PF for the specimen A1. One observes that this is a straight line and that the ZOI experiences a global translation but also a rotation. This measured boundary condition can be applied at each image during the loading phase and then applied to the finite element model of the ZOI to extract directly the precise value of J_{1C}. Figure 6(b) illustrates the evolution of displacements at points E, PE, F and PF up to the maximum load. The error estimated on the displacement is about 0.005mm.

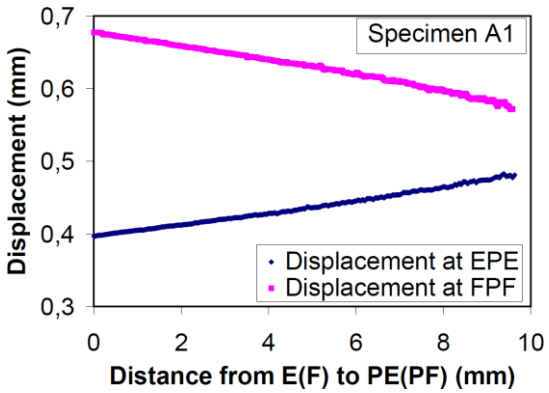

(a) Vertical displacement at maximal load along the boundaries E-PE and F-PF given by DIC

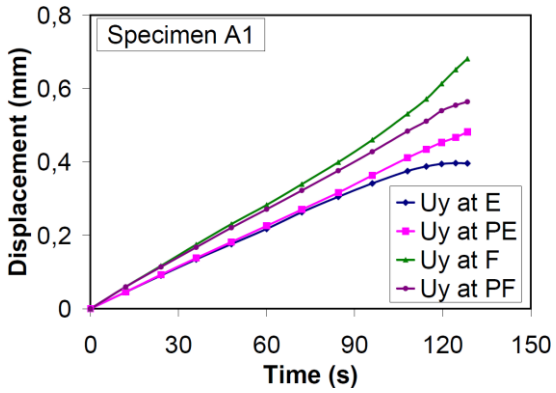

(b) Vertical displacement evolution for points E PE F and PF obtained from DIC

Fig. 6. vertical displacements fields obtained from DIC for specimen A1

4. Numerical simulation

Large strain elastoplastic plane stress analysis was performed using CAST3M [29-31] finite element software in order to evaluate the J_{1C}.

4.1 Mesh and material properties

A special attention is taken to build an appropriate mesh. It consists of a circular part of 10 layers of elements around crack tip. Quadratic 6 and 8 nodes finite elements are used elsewhere. Top and bottom sides are described by 10 elements as we can see in Fig.7 where the mesh has 1358 elements.

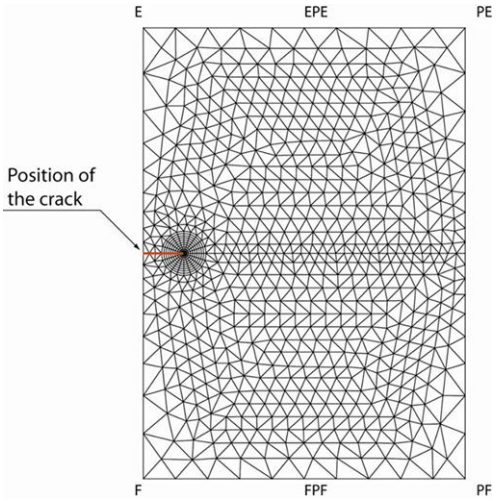

Fig. 7. Mesh used with CAST3M

The size of the simulated zone is 15mm height and 10mm width. The material is considered to be elastoplastic with isotropic hardening. The material data are taken for each experiments form the round bar material characterisation tests done under the same heat treatment history.

4.2 Boundary conditions

Translations and rotations are extracted from the experimental measured displacements histories of lines E-PE and F-PF and applied to the finite element segments EPE and FPF.

4.3 Simulation result and J_{1C} estimation

Fig.8 compares the simulation result of force vs. mean displacement of two top segments of the ZOI with the experimental result for specimen A1 at point A. The agreement is excellent which confirms the quality of the numerical simulation.

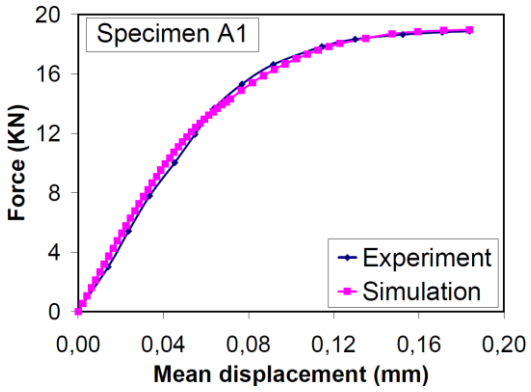

Fig. 8. The force vs. mean displacement of specimen A1 at point A

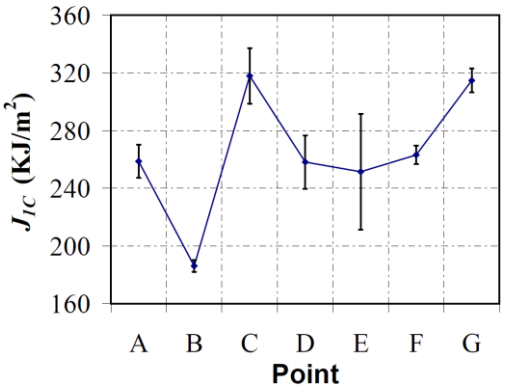

Fig. 9. J_{1C} of 15-5PH at different temperature

After the simulation, J_{1C} is extracted for every specimen at each point using the G_θ method [32][33] which permits to compute the energy release rate for elastoplastic radial loading. For each point (A to G) one has a number of tests available which have all been computed, thus allowing an estimation of the error on the corresponding J_{1C}. The synthesis of the analysis is given in the figure 9.

5. Discussion

The result presented in fig.9 shows that the heat treatment has an influence on J_{1C}. That is t osay heat treatment and metallurgic phase transformation has an influence on the fracture toughness.

If one compares point A and B which are fully martensitic but at different temperature, A has a bigger J_{1C} value than B. The reason is not obvious. The difference is of about 20%, which is not very significant. This should be confirmed by a larger number of experiments.

One now compares the toughness at 200°C but with two distinct metallurgic states: points B (fully martensitic) and C (fully austenitic provided the martensitic transformation is over when the tensile test is performed). J_{1C} for point B is clearly smaller than the one of point C. 15-5PH in austenitic phase is tougher than in martensitic one.

Comparing the toughness J_{1C} of points A and G, the material after a whole cycle heat treatment has a higher fracture toughness than the original material. This should be due to some stable residual austenite in the material after the heat treatment.

For points D、E and F, they all have both martensite and austenite phase whose proportion is given in table.2. Globally the toughness does not seem to be deeply affected during the phase transformation. But the toughness seems to be smaller during the phase transformation than when it is finished or not started.

6. Conclusions

This paper proposed a simple and effective method which mixes Digital Image Correlation (DIC) and finite element numerical simulation to extract the J_{1C} value of 15-5PH at different metallurgical states after typical welding or repair temperature cycles. The effect of thermal history was studied through the analysis of the evolution of toughness of seven points. The effect of the austenite phase transformation on the mechanical behaviour of 15-5PH was studied. The J_{1C} value shows that the pure martensite 15-5PH at room temperature has smaller fracture toughness than after a whole heat treatment, the fracture toughness increase is probably caused by some stable residual austenite. Moreover pure austenite 15-5PH at 200°C has a higher fracture toughness than pure martensite 15-5PH at the same temperature. For the dual phase 15-5PH during the austenite-martensite phase transformation, the austenite phase makes the material more ductile and therefore the fracture toughness is not decreasing significantly in thus dual phase state.

References

[1] Wu, T., 2007. Experiment and numerical simulation of welding induced damage of stainless steel 15-5PH. Ph.D. Thesis, INSA de Lyon, France.

[2] T. Y.Hsu. Martensite transformation and martensite, edition 2. Beijing: Science Press, 1999. 556-564.

[3] Hamata N., Modelisation du Couplage Entre L'elasto-viscoplasticite Ansotherme et la Transformation de Phase D'un Fontr G.S. Ferritique, These de Doctorat de L'universite Paris 6, 1992.

[4] Hashin Z. and Shtrikman S., A variational approach to the theory of the effective magnetic permeability of multiphase materials, Jal. Applied Phys., 33: 3125-3131, 1962.

[5] M.Coret, S.Calloch, A.Combescure, Experimental study of the phase transformation plasticity of 16MND5 low carbon steel under multiracial loading. International Journal of Plasticity, 18 (2002), 1707-1727.

[6] Greenwood, G.W., and Johnson, R.H. The deformation of metals under small stresses during phase transformation, Proc Roy Soc, 283: 403–422, 1965.

[7] Magee C.L. Transformation kinetics, microplasticity and ageing of martensite in Fe-3l-Ni, Ph.D. Thesis, Carnegie Mellon University, Pittsburg, 1966.

[8] J.P.Bressanelli and A.Moskowitz, Effects of Strain Rate, Temperature and Composition on Tensile Properties of Metastable Austenitic Stainless Steels, ASM Trans. Quart. 59, 1966, p.223.

[9] V.F.Zackay, E.R,Parker, D.Fahr and R.Busch, The Enhancement of Ductility in High-Strength Steels, Trans. ASM 60, 1967, p.252.
[10] W.W.Gerberich, P.B.Hemmings, M.D.Merz and V.F.Zackay, Preliminary Toughness Results on TRIP Steel, ASM Trans. Quart.61, 1968, p.843.
[11] Wenyi Yan, Chun Hui Wang, Xin Ping Zhang and Yiu-Wing Mai, Effect of transformation volume contraction on the toughness of super elastic shape memory alloys, Smart Mater. Struct. 11 (2002) 947-955.
[12] W.W.Gerberich, P.B.Hemmings, V.F.Zackay and E.R.Parker, Interactions Between Crack-Growth and Strain-Induced Transformation, Fracture, Chapman and Hall Ltd., London 1969, p.288.
[13] S.D.Antolovich and B.Singh, On the Toughness Increment Associated with the Austenite to Martensite Phase Transformation in TRIP Steels, Met. Trans. 2, 1971, p.2135.
[14] S.R.Pati and M.Cohen, Nucleation of the Isothermal Martensitic Transformation, Acta Met. 17, 1969, p.189.
[15] V.Raghavan and M.Cohen, Measurement and Interpretation of Isothermal Martensitic Kinetics, Met. Trans. 2, 1971, p.2409.
[16] Sun Q-P and Hwang K-C, Micromechanics modelling for the constitutive behavior of polycrystalline shape memory alloys J. Mech. Phys. Solids 1993; 41:1–33.
[17] Hannink R H J, Kelly P M and Muddle B C 2000 Transformation toughening in zirconia-containing ceramics J. Am. Ceram. Soc.83 461-87.
[18] Rice JR. Fracture, vol. 2. Academic Press; 1968. p.191-311.
[19] Begley JA, Landes JD. The J integral as a fracture criterion in fracture toughness: 1971. proceedings, Part II, ASTM STP 514; 1972. p. 1–20.
[20] Yoda, M., 1980, The J-integral fracture toughness for Mode II, Int. J. of Fracture, 16(4), pp. R175-R178.
[21] Christopher D. Wilson, Prabhu Mani. Plastic J-integral calculations using the load separation method for the double edge notch tension specimen. Engineering Fracture Mechanics 75 (2008) 5177-5186.
[22] Dietmar Gross, Thomas Seeling, Fracture mechanics, with an introduction to micromechanics, Springer. 2006. p156-159.
[23] Kumar V, German MD, Shih CF. An engineering approach for elastic–plastic fracture analysis. EPRI Report NP 1931, 1981.
[24] ASTM E1820, Standard Test Method for Measurement of Fracture Toughness, Annual Book of ASTM Standards, ASTM, Philadelphia, PA, 2001.
[25] S. Mguil-Touchal, F. Morestin, M. Brunet, Various experimental applications of digital image correlation method. Laboratoire de Mécanique des Solides, INSA de Lyon.
[26] Thorsten Siebert, Matt J. Crompton, M. Brunet, Application of High Speed Digital Image Correlation for Vibration Mode Shape Analysis. Proceedings of the SEM Annual Conference June 7-10, 2010 Indianapolis, Indiana USA.
[27] H.H. Johnson, Calibrating the electric potential method for studying slow crack growth. Materials research & Standards, 1965; 442-445.
[28] LaMCoS, UMR CNRS 5259, INSA de Lyon, ICASOFT, Digital Image Correlation Software, http://icasoft.insa-lyon.fr/.
[29] Andrei Constantinescu, An introduction to finite elements based on examples with Cast3m. Laboratoire de Mécanique des Solides CNRS UMR 7649, Département de Mécanique, Ecole Polytechnique, 91120 Palaiseau, France.
[30] E. Le Fichoux, Présentation et Utilisation de CASTEM 2000, ENSTA, 1998.
[31] J.S. Fleuret, Prise en main de CASTEM 2000 par l'exemple, CEA Saclay / DRN / DMT / SEMT / LAMS, 1996.
[32] P Destuynder, MDjoua, and S Lescure, Some remarks on elastic fracture mechanics, Journal de Mechanique Théorique et Appliquée, 2:113–135, 1983.
[33] X Z Suo and A. Combescure, Second variation of energy and an associated line independent integral in fracture mechanics. European Journal of Mechanics, A/Solids, 11:609–624, 1992.